Tutor/s

Dr. Lourdes Mestres Vila
Departament de Química Inorgànica i Orgànica
Secció de Química Inorgànica

Grau de Química

Treball Final de Grau

Electroceramic materials for high-energy store capacitors.

Materials electroceràmics per a condensadors d'emmagatzematge d'alta energia.

Carlos Alonso Ayala

June 2022

Universitat de Barcelona

B:KC Barcelona Knowledge Campus
Campus d'Excel·lència Internacional

Nothing in life is to be feared, it is only to be understood. Now is the time to understand more, so that we may fear less.

Marie Curie

I would like to thank my Degree's Final Project supervisor, Dr. Lourdes Mestres, for her dedication, patience, and generosity throughout the development of this project. I am grateful for her knowledge and her working ethic. I would also like to thank Dr. Xavier Vendrell for all the help and support he has given me during these months.

I also want to express gratitude for my lab mates at the Solid State Chemistry group, who helped make this project even more pleasant.

And last but not least, I would like to thank my family and friends for their unconditional love and support.

REPORT

IDENTIFICATION AND REFLECTION ON THE SUSTAINABLE DEVELOPMENT GOALS (ODS)

The research exposed in this report can be associated with the following goals.

- 7. Affordable and clean energy.
- 14. Life below water
- 15. Life on land

Each goal is categorised inside one of the 5Ps. Goal 7 is aligned with Prosperity, while goals 14 and 15 with Planet.

SDG 7 is aligned with Prosperity because of its aim of ensuring a prosperous and fulfilling life for all human beings. The development of capacitors based in BST can collaborate in the achievement of some of the goals of this SDG, such as doubling the global rate of improvement in energy efficiency. Ceramics with better dielectric behaviour can contribute to the development of devices with better energy efficiency. Additionally, the development of better dielectrics can contribute to the improvement of electric devices, and with it, they can be a vector in the universalisation of affordable, reliable and modern energy sources.

SDGs 14 and 15 are aligned with Planet because of their aim of protecting the planet from degradation. Lead-free ferroelectrics can prevent marine and land pollution by eliminating the generation of lead-containing waste, whether it is generated during the production of the material or during the treatment of electronic waste that contains lead-based electroceramics.

CONTENTS

1. SUMMARY

Dielectric materials such as electroceramics have a wide use in electronical devices, like capacitors. Lead zirconate titanate (PZT) is the most used electroceramic. However, lead toxicity has raised concerns about its use, due to its capacity to endanger the health and the environment. For this reason, since the early 2000s there has been substantial research on lead-free electroceramics that could present electrical properties similar to those of PZT.

Materials based in $BaTiO_3$ (BTO) have attracted great interest as possible substitutes of PZT. Like PZT, BTO presents dielectric behaviour and perovskite structure. However, its electrical properties are not as good as the ones described for PZT. For this reason, numerous researchers have studied derivatives of BTO in which doping elements improve its electrical behaviour.

In this project, $Ba_{1-x}Sr_xTiO_3$ (BST) is proposed as an alternative to PZT. To do so, various BST compositions have been prepared through solid-state reaction. Characterisation by XRD confirmed the synthesis of single-phase BST compounds and the variation of unit cell parameters, which correspond with the introduction of Sr in the perovskite structure of BTO. In addition, distribution of elements across the material was analysed with EDS. The morphology of the ceramics was studied with SEM. Moreover, the dielectric behaviour of BST compounds was characterised by EIS. It was observed that BST compounds with Sr content ranging between 50 % and 70 % do not present phase transition at temperatures between 313 K and 473 K. In addition, BST low dielectric loss, along with its limited permittivity variability in the studied temperature range, confirm BST feasibility as a candidate to be used in capacitors.

Keywords: barium strontium titanate, lead-free dielectrics, solid-state reaction, ceramics, perovskite, electrical properties.

2. RESUM

Els materials dielèctrics, com ara les electroceràmiques, tenen un ampli ús en dispositius electrònics com els condensadors. El titanat zirconat de plom (PZT) és l'electroceràmica més utilitzada. No obstant això, la toxicitat del plom ha generat preocupacions sobre el seu ús, a causa de la seva capacitat de posar en perill la salut i el medi ambient. Per aquest motiu, des de principis dels anys 2000, hi ha hagut molta investigació sobre dielèctrics sense plom que podrien presentar propietats elèctriques similars a les del PZT.

Els materials basats en $BaTiO_3$ (BTO) han despertat un gran interès com a possibles substituts del PZT. Tal com passa amb el PZT, BTO presenta comportament dielèctric i estructura de perovskita. Tanmateix, les seves propietats elèctriques no són tan bones com les descrites per a PZT. Per aquest motiu, nombrosos investigadors han estudiat derivats de BTO en què elements dopants milloren el seu comportament elèctric.

En aquest projecte es proposa $Ba_{1-x}Sr_xTiO_3$ (BST) com a alternativa a PZT. Per fer-ho, s'han preparat diverses composicions de BST mitjançant reacció en estat sòlid. La caracterització amb XRD va confirmar que els compostos BST preparats són de fase única i que la variació dels paràmetres de cel·la es correspon amb l'entrada d'estronci en l'estructura perovskita del BTO. A més, la distribució dels elements en el material es va analitzar amb EDS. La morfologia de la ceràmica es va estudiar amb SEM. Addicionalment, el comportament dielèctric dels compostos BST es va caracteritzar per EIS. Es va observar que els compostos BST, amb contingut en Sr que oscil·la entre el 50 % i el 70 %, no presenten transició de fase a temperatures entre 313 K i 473 K. A més, les baixes pèrdues dielèctriques i la poca variabilitat de la permitivitat d'aquests materials en el rang de temperatures estudiat els converteix en candidats a ser usats en condensadors.

Paraules clau: titanat de bari i estronci, dielèctrics sense plom, reacció en estat sòlid, ceràmica, perovskita, propietats elèctriques.

3. INTRODUCTION

Capacitors are devices capable of storing electrical energy when an electric field is applied. This property is provided by capacitance, which is capability of a capacitor to store electric charge. The charge in a capacitor is stored between two electrodes separated by a dielectric material, such as ceramics. Some dielectrics are also piezoelectric. These are materials that generate stress when an electric field is applied or generate an electric field when stress is applied. A type of piezoelectric material are ferroelectrics, which possess permanent polarization once the applied electric field is removed.

Ferroelectricity was not discovered until 1920,[1] when student Joseph Valasek was studying the piezoelectricity of Rochelle salt (potassium sodium tartrate tetrahydrate).[2] Previous research indicated anomalous electric behaviour of Rochelle salt when electric field or stress was applied. In his work, Valasek proved permanent polarization and 'memory effect' known as hysteresis to be present in Rochelle salt.

Valasek's discovery aroused curiosity amongst his colleagues. In 1935, Paul Scherrer and Georg Busch discovered ferroelectricity in KH_2PO_4 to be present at temperatures below – 150 °C.[3]

However, the applications of the ferroelectrics discovered at that time were limited: both Rochelle salt and KH_2PO_4 were soluble in water and had poor mechanical behaviour. It was not until 1946 that a polycrystalline ceramic like $BaTiO_3$ (BTO) was found to exhibit ferroelectricity.[4] Its great properties soon made BTO a candidate to be used in electrical devices.[5] Research in the ferroelectric properties of other perovskites followed the discovery of ferroelectricity in BTO. The most prominent discovery was found in lead zirconate titanate (PZT), with general formula $PbZr_xTi_{1-x}O_3$, which quickly replaced as the main ferroelectric, due to its better electric properties. PZT would later become the most used piezoelectric. But concerns regarding toxic substances such as Pb encouraged the European Union to pass legislation in 2002 regarding the regulation of their use. In response, a group of Japanese researchers reported in 2004 the extraordinary properties of $(K,Na)NbO_3$-based ceramics, not too dissimilar to those of PZT. Their work triggered the interest of research in Pb-free ceramics.[6,7]

3.1. THEORETICAL FRAMEWORK

3.1.1. Solid-state reaction

The solid-state reaction, also known as ceramic method, is the most common preparative strategy for polycrystalline inorganic solids, such as ternary oxides, sulphides or carbonates.[8] It is a reaction involving two non-volatile solids. Due their inherent stiffness, reactions between solids at room temperature are not labile. For that reason, high temperatures, usually between 1000 °C and 1500 °C, are required to increase their almost inexistent mobility, and therefore produce the desired substance.

In the case of solid-state reactions that occur without the formation of melt, the mechanism starts by the reaction at the points of contact between the solid reactants. It is then followed by the diffusion of the product through the volume of the mixture. As this new phase grows, the number of contact points between reactants reduces and, consequently, diffusion paths become longer, causing the decrease of the reaction rate. Eventually, the formation of the product is stopped, obtaining a heterogeneous product. To complete the reaction, it is recommended to grind and set up another thermal treatment repeatedly until a single-phase product is formed.

3.1.2. Perovskite structure

Many dielectric compounds, such as $BaTiO_3$, are based on a perovskite structure. A perovskite is a material consisting of a crystal structure of general formula ABX_3, where A and B are two different cations and X is usually oxygen. Its name comes from mineral perovskite, which is made of $CaTiO_3$. The mineral was discovered in 1839 by German mineralogist Gustav Rose in the Ural Mountains and named after Russian count Lev Perovski. Perovskites exhibit a wide variety of properties depending on their composition, including ferroelectricity, superconductivity, semiconductivity, ferromagnetism or colossal magnetoresistance.[9,10]

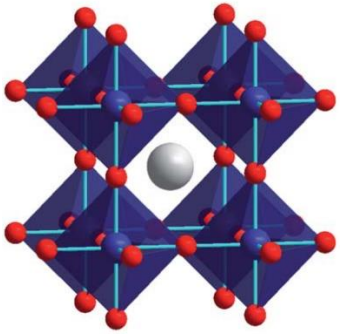

Figure 1. *Cubic perovskite structure, where the grey sphere represents A, blue spheres B and red spheres X. (image from King et al., ref. 10)*

The cubic structure seen in Figure 1 is best defined as a net of BX_6 octahedrons linked through each of their six vertices. B cation, with coordination number 6, is found in the vertices and A cation, with coordination number 12, is in the centre of cubic cell, so that the ionic radius $r_A > r_B$. X anion occupies the edges of the cell. Nevertheless, cubic is the ideal crystal system. Therefore, perovskites could present distortions that lower the symmetry. They can be caused by:

- Jahn-Teller effect: distortion of the octahedrons.
- Displacement of A and B from the equilibrium position.
- Rotation or inclination of BX_6 octahedrons due to the insertion of A' cations in A-site, so that the ionic radius $r(A') < r(A)$.

The quantification of these distortions and stability of the perovskite crystal structure is defined by Goldschmidt's tolerance factor, t:

$$t = \frac{r_A + r_B}{\sqrt{2}(r_B + r_X)} \qquad (1)$$

where r_A, r_B and r_X are the ionic radii of A, B and X respectively. For instance, $t = 1$ for cubic structure and $t < 0.85$ for unstable distorted perovskite structures. Distortion can be found in compounds such as $BaTiO_3$, due to Ti being a little smaller than supposed for its octahedral site, causing a displacement of cations towards one of the corners of the octahedron. Consequently, there is a net dipole moment. This high polarizability, along with a high permittivity, is responsible for ferroelectricity.

3.1.3. Electric properties of ferroelectric materials

3.1.3.1. Dielectric materials

Dielectric materials, like the ones used as capacitors, are electrical insulators. They are uncapable of conducting electricity but can be polarised by an applied electric field. This characteristic is caused by the unavailability of electrons to flow loosely through the material. Instead, charges can only do a slight reorganisation from their equilibrium position, creating an internal electric field opposed to the applied field. This phenomenon, known as polarization, disappears when the field is removed. However, ferroelectric materials are a special type of due to the maintenance of a big polarization once the field has been removed.

This type of material is also defined by two main properties: high dielectric strength and low dielectric loss. Dielectric strength is capacity to undergo an applied electric field without being degraded to an electrically conducting material. And, for an alternating current (AC), dielectric loss is a component of electrical energy which is lost in the form of heat in a dielectric material.

Capacitance is the amount of charge that can be stored in a capacitor. With vacuum between its plates, it depends on the dimensions of the device. It is defined as

$$C_0 = \frac{\varepsilon_0 A}{d} \tag{2}$$

where A is the area of the plates and d the distance between the plates.

When a potential difference V is applied between the plates, the charge stored on the capacitor is

$$Q_0 = C_0 V \tag{3}$$

And when the same potential difference V is applied and vacuum between the plates is replaced by a dielectric medium, the charge stored is now Q_1 and the capacitance C_1. Therefore, the relative permittivity ε_r is

$$\varepsilon_r = \frac{C_1}{C_0} \tag{4}$$

The relative permittivity estimates the degree of polarization than takes place in the material. For air, $\varepsilon_r \approx 1$. For most ionic solids, $5 \leq \varepsilon_r \leq 10$. For ferroelectric materials such as $BaTiO_3$, $10^3 \leq \varepsilon_r \leq 10^4$.[11]

The macroscopic dielectric polarization ***P*** of a pure dielectric material is related to electric field ***E*** by

$$\boldsymbol{P} = \varepsilon_0 X_e \boldsymbol{E} \quad (5)$$

where X_e is the electric susceptibility, which is related to the relative permittivity ε_r by $X_e = \varepsilon_r - 1$, taking $X_e = 0$ in the case of vacuum.

The polarizability α of the dielectric material is defined by

$$\boldsymbol{p} = \alpha \boldsymbol{E} \quad (6)$$

where $\boldsymbol{p}$ is the dipole moment induced by the local electric field $\boldsymbol{E}$. The polarizability can have up to four components, so that

$$\alpha = \alpha_e + \alpha_i + \alpha_d + \alpha_s \quad (7)$$

where

- α_e is the electronic polarizability. It is found in all solids, due to the displacement of the electron cloud of atoms.
- α_i is the ionic polarizability. It is the main component in ionic solids, caused by the separation of oppositely charged ions.
- α_d is the dipolar polarizability. It occurs in materials with a permanent electric dipole.
- α_s is the space charge polarizability. It happens in materials with a non-homogeneous charge density, due to some relatively long-range migration experienced.

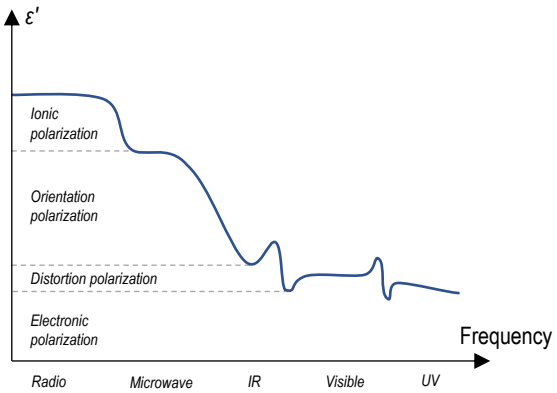

Figure 2. *Contribution of each polarizability component to relative permittivity depending on the frequency.*
(adapted from Izgorodina, E. I. *et al.*, *Phys. Chem. Chem. Phys.*, **2009**, *11*, 2452)

As can be seen in Figure 2, when the frequency of the AC applied is high, the contributions of α_d and α_s are not present, as happens in good dielectrics. Only α_e and α_i are involved because of the speed of these processes.

3.1.3.2. Ferroelectric materials

Ferroelectric materials are dielectric materials capable of retaining a certain amount of polarization after the applied electric field has been removed. Because of this, they are distinguished by their large permittivities.

The relation of polarization and thus stored charge with the applied potential difference seen on Equation 3 for dielectric materials does not hold for ferroelectricity. Instead, a non-linear behaviour is observed, and is described in a hysteresis loop, as seen on Figure 3.

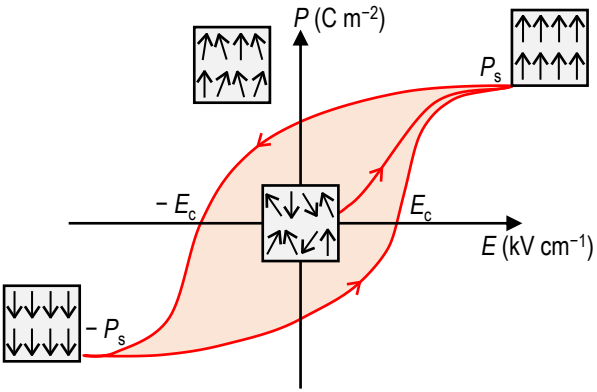

Figure 3. *Hysteresis loop of a ferroelectric material.*

In a ferroelectric material, when the electric field strength E is increased, polarization also increases until reaching a maximum polarization, also known as saturation polarization, P_s. When P_s is reached, electric dipoles are parallelly oriented. After P_s, when E is removed, polarization does not drop to zero, but a remanent polarization P_r is retained. To obtain zero polarization, a reverse field, known as coercive field E_c, is required.

Ferroelectricity is commonly observed at low temperatures. Otherwise, spontaneous polarisation would not arise. A ferroelectric phase loses its properties, becoming a paraelectric phase, at temperatures greater than Curie temperature, T_C. Nevertheless, at $T > T_C$, the material will still have a large permittivity, as given by the Curie-Weiss law:

$$\varepsilon_r = \frac{C}{T - \theta} \tag{8}$$

where C is the Curie constant and θ the Curie-Weiss temperature. Usually, $T_C \approx \theta$ and consequently, $\varepsilon_r \rightarrow \infty$. However, at the ferroelectric-paraelectric phase transition, ε_r takes a characteristic maximum value.

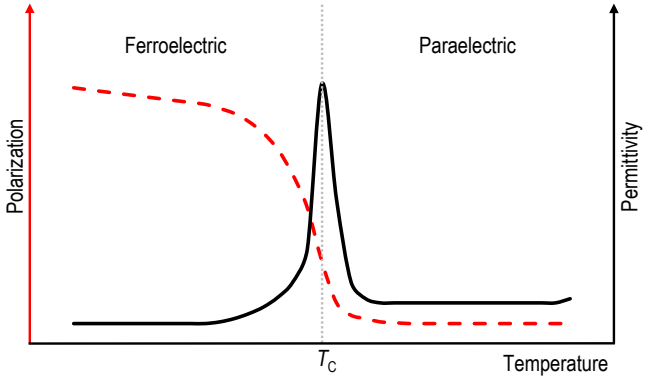

Figure 4. *Permittivity and polarization at the phase transition.*

Figure 4 describes a normal phase transition. A wider peak would describe a diffuse phase transition. In materials known as relaxor ferroelectrics, a wide peak would be dependent of the frequency.

3.1.4. Barium strontium titanate

Barium strontium titanate (BST), with general formula $Ba_{1-x}Sr_xTiO_3$, has a perovskite structure, resulting from the Ba^{2+}-site doping of $BaTiO_3$ with Sr^{2+}. The crystal structure of BST depends on its stoichiometry of the BST, hence different compositions of BST will have different phase transition behaviours. In other words, BST compounds have a structure halfway through $BaTiO_3$, a ferroelectric at room temperature due to its tetragonal symmetry, and $SrTiO_3$, a paraelectric at room temperature due to its cubic symmetry.

Consequently, BST compounds with higher content of Sr ($x > 0.3$) are cubic at room temperature and present paraelectric behaviour, whereas compounds with lower Sr content ($x < 0.3$) are tetragonal at room temperature and present ferroelectric behaviour.[12] In other words, increasing the content of Sr decreases the Curie temperature T_C at which takes place the tetragonal-cubic transition, as represented in Figure 5. For instance, $BaTiO_3$ has a $T_C = 120$ °C, BST30 has a $T_C = 34$ °C and BST60 has a $T_C = -66$ °C.[13,14] These changes are provoked by the shrinkage in the unit cell volume caused by the introduction of Sr^{2+} in the cell, which has a smaller ionic radium than Ba^{2+}.[15]

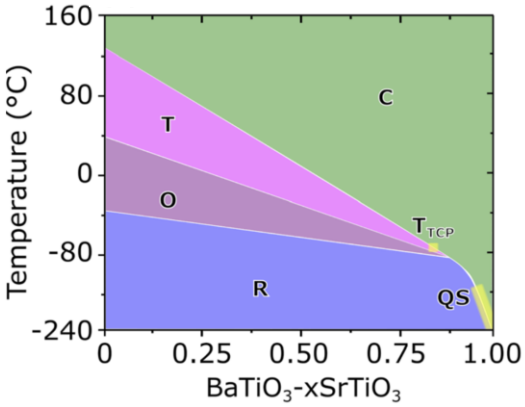

Figure 5. *Phase diagram of $Ba_{1-x}Sr_xTiO_3$, where R is the rhombohedral, O the orthorhombic, T the tetragonal and C the cubic phase*.

(image from Acosta, M. *et al.*, *ref. 6*)

BST generally presents a normal phase transition. However, impurities or an uneven distribution of Ba^{2+} and Sr^{2+} can lead to a diffuse[16] or a relaxor[17] phase transition.

3.2. CHARACTERISATION TECHNIQUES

3.2.1. Infrared spectroscopy

Infrared spectroscopy is a technique used for the structural determination of compounds. It is based in the excitation of vibrational states at a precise wavelength in the IR region. For this reason, its absorption is related to the structure of the chemical species.

IR measurements were carried out with a Thermo Nicolet iS5 spectrometer available at the *Secció de Química Inorgànica* of the *Universitat de Barcelona*, with wavenumbers in the range of 500 and 4000 cm^{-1}.

3.2.2. X-ray diffraction

X-ray diffraction (XRD) is the most common technique for the structure characterisation of crystalline species. It is a non-destructive technique based in the scattering that X-ray beams suffer when they collide over the periodic structure of a crystal, which consists in the sum of crystallographic planes. These parallel planes diffract the incident beam in multiple directions. The interference between the diffracted waves generates a diffraction pattern, which is the conjunction of constructive and destructive interferences, corresponding to the maximums and

minimums of the pattern respectively. Nevertheless, only constructive interferences are energetic enough to be measured by the detector, as can be seen in Figure 6.

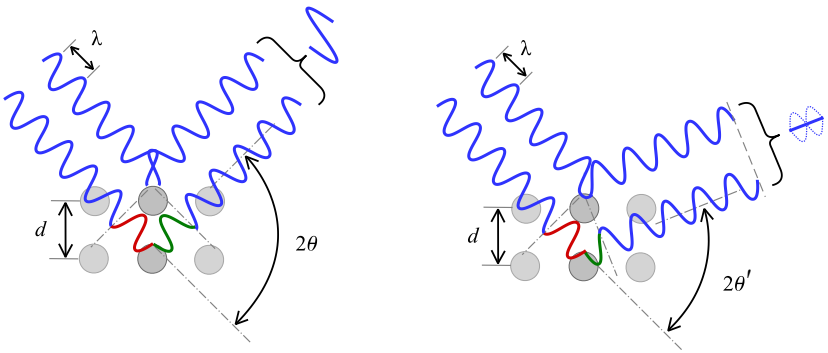

Figure 6. *Diagram of Bragg's law. On the left, the diffracted waves are in phase (constructive interference). On the right, the diffracted waves are out of phase (destructive interference).*
(Cdang, 8/3/2011 via Wikimedia Commons, Creative Commons Attribution)

In the early 20th century, W. H. Bragg and his son W. L. Bragg proved that, for monochromatic radiation of wavelength in the atomic scale, diffraction showed the same mirror-like behaviour as specular reflection. Therefore, for a constructive interference, Bragg's law is satisfied, so that

$$2d \sin\theta = n\lambda \qquad \forall\, n \in \mathbb{N} \tag{9}$$

where d is the interplanar spacing, θ the diffraction angle and λ the wavelength.

Due to the mirror-like behaviour of diffraction observed by Bragg, it can be derived that crystal planes diffract the X-rays with the same angle as the incident beam. This angle varies with the interplanar spacing, which is an intrinsic property of the crystal, related to the unit cell parameters.

XRD studies were carried out at *Centres Científics i Tecnològics de la Universitat de Barcelona* with PANalytical X'Pert PRO MPD alpha1 diffractometer, with a Ge (111) monochromator. The radiation used was the K_α line of Cu (1.5406 Å) at 45 kV and 40 mA, and the diffraction pattern was registered for 2θ angles from 4º to 100º, with a measuring time of 100 seconds. The diffraction patterns were studied with the X'Pert HighScore50 software. The samples were compared with *Powder Diffraction File* (PDF) patterns of the *International Centre for Diffraction Data* (ICDD) database.

3.2.3. Electrochemical impedance spectroscopy

Electrochemical impedance spectroscopy (EIS) is a technique used in the characterisation of the electrical properties of materials. It is based on the application of an electric field to a dense pellet of the compound of interest. Frequency and temperature are altered to study their correlation with magnitudes such as permittivity.

Taking into account that measurements are carried out in AC, the applied voltage is

$$V(t) = V_0 \sin \omega t = V_0 e^{i\omega t} \quad (10)$$

and the response of the material is dependent on the frequency of the external field, so that

$$I(t) = I_0 \sin(\omega t + \delta) = I_0 e^{(i\omega t + \delta)} \quad (11)$$

where i is the imaginary unit, $i^2 = -1$, ω is the angular frequency and δ the loss angle, which is the time delay between the applied voltage and its response.

The sample input and output can be related through a magnitude called impedance,[18,19] so

$$Z(t) = \frac{V(t)}{I(t)} = Z_0 e^{i\delta} \quad (12)$$

where $Z_0 = V_0 / I_0$. Since impedance Z is a complex magnitude, it can also be expressed in the form of a vector in the complex plane:

$$Z = R + iX \quad (13)$$

where R is the resistance and X the reactance. In AC, capacitance is also a complex magnitude, which is related to impedance Z. In this case, the complex capacitance can be defined as

$$\widetilde{C} = \frac{1}{i\omega Z} \quad (14)$$

Permittivity will also be expressed as a complex magnitude which is related to complex capacitance $\widetilde{C}$ and therefore to impedance Z:

$$\varepsilon = C_0 \widetilde{C} \quad (15)$$

Consequently, permittivity can be defined analogously to Equation 12

$$\varepsilon = \varepsilon' + i\varepsilon'' \quad (16)$$

where the real part is the permittivity, and the imaginary part is the dielectric loss. Considering the relationship between permittivity and impedance, both components of permittivity will also be related to the loss angle δ by $\varepsilon' = \mathrm{Re}(\varepsilon) = |\varepsilon| \cos \delta$ and $\varepsilon'' = \mathrm{Im}(\varepsilon) = |\varepsilon| \sin \delta$. In other words, a dielectric loss factor can be determined for a known frequency of the AC applied to the sample

$$\tan \delta = \frac{\varepsilon''}{\varepsilon'} \quad (17)$$

This magnitude quantifies the quality of the material as an insulator. As can be seen in Figure 7, when $\delta = 90°$, the contribution of ε'' is zero, meaning that the material is a perfect dielectric. As the frequency increases, the loss angle decreases, meaning that dielectric loss increases and permittivity decreases.

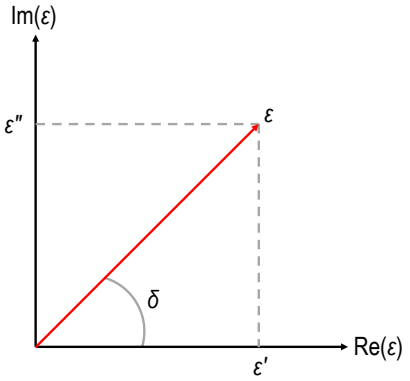

Figure 7. *Permittivity in the complex plane.*

The electrical characterisation of a porous sample would not allow the correct analysis of the material, due to the contribution of the permittivity of air. To avoid this situation, the sample must have a high relative density.

Electrochemical impedance spectroscopy measurements were performed with an HP 4192A impedance analyser available at the *Química de l'Estat Sòlid* group of the *Universitat de Barcelona*. The study of each sample was carried out at temperatures ranging between 40 °C and 200 °C, and frequencies between 0.01 kHz and 10 000 kHz.

3.2.4. Scanning electron microscopy

Scanning electron microscopy (SEM) is the most used electron microscope-based characterisation technique. It consists in the irradiation of an electron beam on the surface of a sample. Due to its large depth of field, SEM can obtain three-dimensional images of the specimen.

Another advantage with respect to optical microscopy is its magnification range, placed between 10 and 100 000×. Thanks to it, materials can be characterized at the micrometric to nanometric scale.[20]

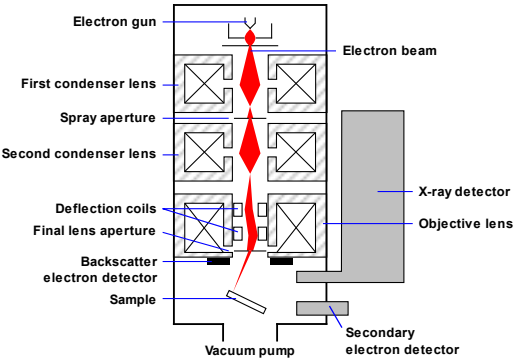

Figure 8. *Schematic representation of a SEM.*
(Steff, 3/3/2010 via Wikimedia Commons, Creative Commons Attribution)

A SEM has two principal components: an electron column and a control console. As shown in Figure 8, the electron column is based on an electron gun, two or more lenses, a deflection system, and a detector. The column is connected to a vacuum pump that can reduce the pressure to an order of magnitude between 10^{-2} and 10^{-8} Pa. The electron gun accelerates electrons at voltages between 1 and 30 kV. It can be based on a thermoionic tip (either made of tungsten or a single crystal of LaB_6) or a field emission tip made of tungsten. Due to the size of the tip, electromagnetic lenses are required to demagnify the image. These lenses, consisting of an electromagnet made of copper coils and soft iron poles, allow the placement of a smaller and more focused electron beam on the specimen. A smaller electron spot means that the scanned image is generated point by point. To scan the entire surface of the sample, a deflection system is used, moving the electron spot along a line, and then another line below continuously until the sum of each spot forms a rectangular raster on the specimen surface.

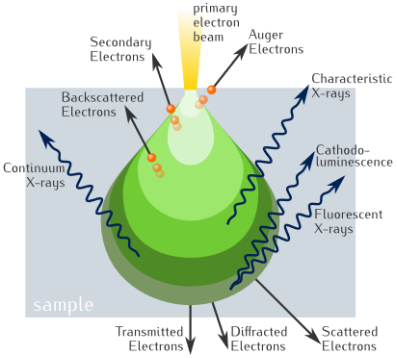

Figure 9. *Scheme of the electron-sample interaction in SEM and the different types of signals generated.*
(Ponor, 28/8/2020 via Wikimedia Commons, Creative Commons Attribution)

The interaction between the incident beam and the sample generates different types of signals, as seen on Figure 9. In this project, only secondary electrons (SE) and backscattered electrons (BSE) were analysed. SE are generated from the collision between the incident electrons and the external electrons of the atoms of the surface. These electrons have low energy, and their trajectory can therefore be deviated. For this reason, SE give topographical information of the surface, providing a three-dimensional image of the sample. SE are useful for the determination of the morphology of samples.

On the other hand, BSE are generated from the elastic collision of the incident electrons and the nucleus of the atom. These electrons have high energy, but depending on the atomic number, the energy varies: a greater atomic number generates electrons with greater energy. For this reason, BSE give information of the mass of the atoms in the sample, allowing the differentiation of the phases present in the sample. However, opposite to SE, a three-dimensional image cannot be obtained, due to the depth of the atoms where the signal is generated.

SEM was performed at *Centres Científics i Tecnològics de la Universitat de Barcelona* with a JEOL JSM-6510 microscope.

3.2.5. Energy dispersive X-ray spectroscopy

Energy dispersive X-ray spectroscopy (EDS) is a technique based in the emission of X-rays by atoms of the sample after having been bombarded with an energetic electron beam. This emission is caused by the decay of electrons from the valence shell. The emission characterises the energy gap between the shells of the atom. Since this electron transition is characteristic of each element, EDS allows the determination of the composition of the sample.

4. OBJECTIVES

The main objective of this project is to analyse the electrical properties of strontium-doped barium titanate. To achieve this goal, the following objectives ought to be fulfilled.

- Optimisation of the thermal treatment conditions.
- Identification of the crystal structure of the BST compounds.
- Study of the morphology and composition of the ceramics.
- Study of the dielectric behaviour of BST compounds at different temperatures and frequencies.
- Establishment of the effect of varying the strontium content in the crystal structure, electrical properties and morphology.

5. EXPERIMENTAL SECTION

Three different compositions of $Ba_{1-x}Sr_xTiO_3$, which from now on will be referred to as BST*x*, have been synthesised: $Ba_{0.5}Sr_{0.5}TiO_3$ (BST50), $Ba_{0.4}Sr_{0.6}TiO_3$ (BST60) and $Ba_{0.3}Sr_{0.7}TiO_3$ (BST70). Additionally, non-strontium-doped barium titanate ($BaTiO_3$) was prepared. Their synthesis was done with the use of the materials listed in Table 1.

	Raw material	Commercial reference	Purity [%]	Molar mass [g mol^{-1}]	Powder colour
1	$BaCO_3$	Sigma-Aldrich 237108	≥ 99	197.34	White
2	$SrCO_3$	Panreac 141306	98	147.63	White
3	TiO_2	Sigma-Aldrich 14021	≥ 99	79.87	White

Table 1. Raw materials used on BST synthesis.

Each of the aforementioned compounds were synthesised through a solid-state reaction.

$$1 - x\ BaCO_3\ (s) + x\ SrCO_3\ (s) + TiO_2\ (s) \xrightarrow{\Delta} Ba_{1-x}Sr_xTiO_3\ (s) + CO_2\ (g)$$

Measuring the weight of the reagents becomes the critical point of the procedure so as to obtain the desired stoichiometry of each species. To achieve this, a thermal treatment is required for each reagent before the solid-state reaction, with the aim of removing any undesired traces of water or carbonate that could add uncertainty to the weight of the reagent. Barium and strontium carbonates were dehydrated in a muffle furnace at 220 °C for 24 hours, while titanium dioxide was decarbonised and dehydrated at 900 °C for 8 hours, as seen on Figure 10.

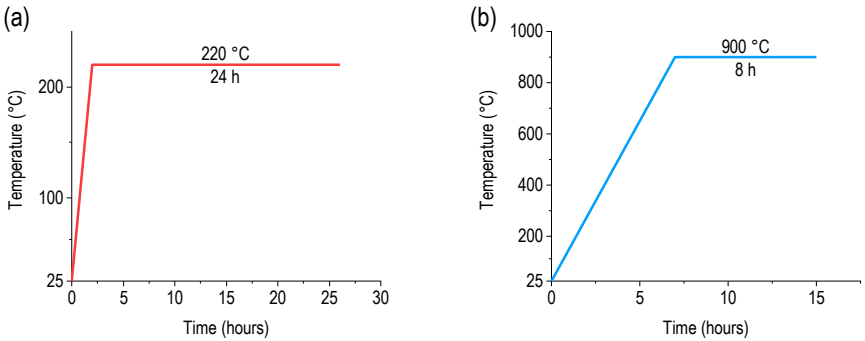

Figure 10. *Heating curves of the thermal treatments followed for $BaCO_3$ and $SrCO_3$ (a) and for TiO_2 (b).*

Once the pre-treatments were completed, reagents were weighted with ± 0.1 mg precision until reaching the stoichiometrically required quantity for the synthesis of 5 g of the desired compound. The mixture was then homogenised with ethanol in an agate mortar. Once ethanol evaporated, the obtained powder was turned into 1 g pellets after applying a pressure of ≈ 320 MPa. The objective of turning the powder into pellets is to increase the contact area of grains, which results in a greater diffusivity and therefore promoting an effective synthesis. The remaining powder was used to determine the IR spectrum of the mixture.

Calcination is the upcoming step. It is the thermal treatment in which the synthesis of the desired compound takes place. Its mechanism consists in the thermal decomposition of both $BaCO_3$ and $SrCO_3$ and their successive diffusion across the pellet volume.

$$BaCO_3\,(s) \xrightarrow{\Delta} BaO\,(s) + CO_2\,(g)$$

$$SrCO_3\,(s) \xrightarrow{\Delta} SrO\,(s) + CO_2\,(g)$$

$$1 - x\,BaO\,(s) + x\,SrO\,(s) + TiO_2\,(s) \xrightarrow{\Delta} Ba_{1-x}Sr_xTiO_3\,(s)$$

The 1 g pellets were introduced in a furnace. The temperature selected for the calcination is 1250 °C. This plateau was maintained for 4 hours, ensuring a quantitative decomposition of carbonates and synthesis of either BTO or BST. As can be seen on Figure 11, the plateau was reached after increasing the temperature at a relatively slow rate of 120 °C/h, to reduce the possibility of generating a secondary phase. The cooling was done at the same rate for the same reason.

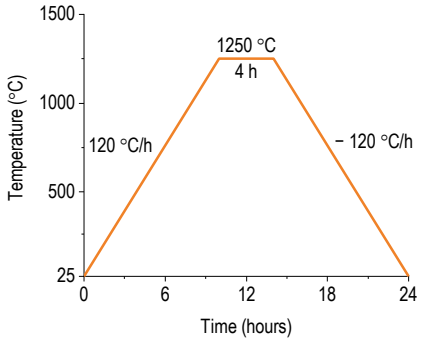

Figure 11. *Thermal treatment scheme of the calcination process.*

The product obtained from this thermal treatment was characterised by IR spectroscopy to guarantee the decomposition of carbonates.

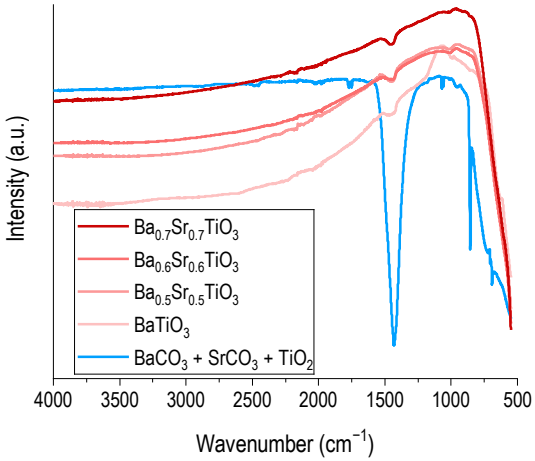

Figure 12. *IR spectra of the reagents mixture before calcination and after calcination.*

As can be seen on Figure 12, absorption bands were observed at 1750 cm^{-1}, 1410 cm^{-1}, 1060 cm^{-1}, 860 cm^{-1} and 690 cm^{-1}. The band at 1750 cm^{-1} is assigned to the C-O asymmetrical stretching (v_1 + v_4). The band at 1410 cm^{-1} is assigned to the C-O asymmetrical stretching (v_3). The band at 1060 cm^{-1} is assigned to the C-O symmetrical stretching (v_1). The band at 860 cm^{-1} is assigned to the CO_3^{2-} out-of-plane deformation (v_2). And the band at 690 cm^{-1} is assigned to the CO_3^{2-} in-plane deformation (v_4).[21] Nevertheless, this last band could also be associated with the presence of Ti-O bonds.[22] As can also be seen on Figure 12, absorption

bands disappear once the mixture has gone through calcination, confirming the decomposition of carbonates.

The pellets that underwent calcination were grinded. A part of the powder was analysed with XRD to confirm the obtention of the desired product. And the rest was turned into 0.5 g and 0.15 g pellets after applying ≈ 320 MPa and ≈ 720 MPa pressure respectively. The pellets were prepared for the next thermal treatment, which is sintering. Its aim is to obtain a denser pellet, due to high density being a requirement for a correct electrical characterisation. To achieve this, a 1350 °C temperature is maintained for 4 hours. As can be seen on Figure 13, the plateau was reached after increasing the temperature at a relatively slow rate of 120 °C/h, to reduce the possibility of generating a secondary phase. The cooling was done at the same rate to avoid the cracking of the pellet due to thermal shock.

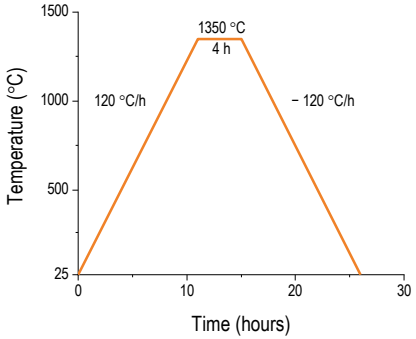

Figure 13. *Thermal treatment scheme of the sintering process.*

Once the sintering process is finished, a measurement of the density of the obtained pellets is done. To do so, pellets are weighed with ± 0.1 mg precision and their height and diameter are measured with a calliper. Assuming that the pellet with height h and diameter d has a cylindrical shape, its density is

$$\rho = \frac{m}{V} = \frac{m}{\pi r^2 h} = \frac{4m}{\pi d^2 h} \tag{18}$$

where m is the mass of the pellet. The densest pellet was used for the electrical characterisation of the compound. If the relative density of the pellet was not high enough, a second sintering process was performed, increasing the temperature 50 °C with respect to the previous sintering.

	Compound	BTO	BST50	BST60	BST70
Relative density [%]	Sintered at 1350 °C	81	81	69	72
	Sintered at 1400 °C	—	—	76	73

Table 2. Relative density of the sintered pellets.

The relative density shown in Table 2 is the ratio between the density obtained and the theoretical density. The theoretical density is obtained after the XRD characterisation of the sintered sample. This value can be obtained from the calculation of the unit cell parameters, which requires the assignment of each peak with a Miller index.

When good density is obtained, the surface of the densest pellet is polished with an abrasive sheet of P800 granulometry. To perform the electrical characterisation, the pellet requires two electrodes. To do so, the pellet is covered with a thin film of gold thanks to sputtering deposition. Pellets were coated with a Quorum SC7620 Sputter Coater located at the *Caracterització Elèctrica de Materials i Dispositius* (CEMAD) group from the *Departament de Física* at the *Universitat Politècnica de Catalunya*. Once the pellet is coated, its border has to be polished, in order to separate the two electrodes.

6. RESULTS AND DISCUSSION

Barium titanate and barium strontium titanate compounds were characterised by means of XRD, SEM, EDS and EIS.

6.1. X-RAY DIFFRACTION

XRD was carried out with the aim of obtaining information regarding the phase and the crystal structure of compounds. Information about the crystal structure derived from the diffraction pattern is obtained when it is compared to the patterns available in the *Powder Diffraction Files* (PDF) of the *International Centre for Diffraction Data* (ICDD) database. Taking into account that BST consists in an A-site doping of BTO, the diffraction patterns of the doped compounds were compared with the information available at the PDF 00-005-0626. Additionally, they were also compared with PDF 00-039-1395, corresponding to BST50.

The diffraction pattern in Figure 14 shows that the BTO compound is a single-phase product that has tetragonal symmetry at room temperature.

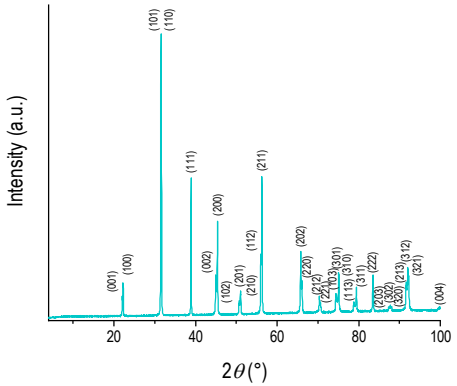

Figure 14. X-ray diffraction pattern of BTO and its *Miller indices assignment.*

The results of the XRD characterisation of each barium strontium titanate compound are found in Figure 15. It can be seen that all of the sintered products consist in a unique phase perovskite.

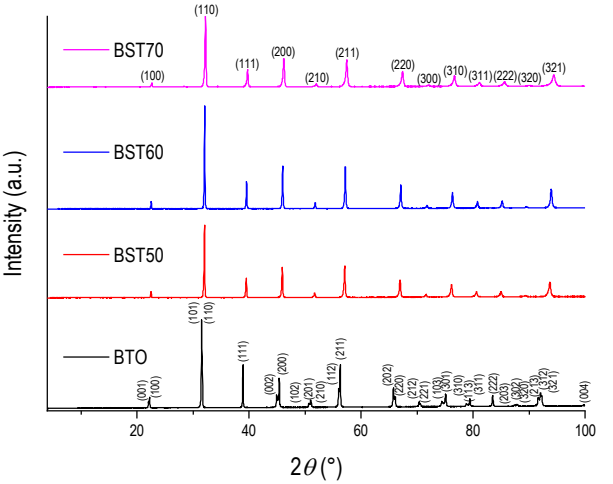

Figure 15. X-ray diffraction pattern of BTO and BST and its *Miller indices assignment.*

As Sr^{2+} is introduced into the BTO structure, all the doublets and triplets corresponding to tetragonal symmetry coalesce into symmetrical peaks associated with cubic symmetry.

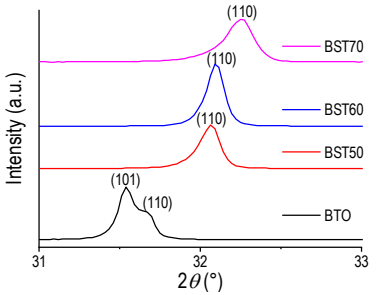

Figure 16. *Zoomed X-ray diffraction pattern at the 31° ≤ 2θ ≤ 33° region.*

Figure 16 shows the displacement of BST peaks. Peaks shift to higher diffraction angles when the Sr content is increased, indicating that unit cell volume decreases when Sr is added. This is caused by Sr^{2+} having a smaller ionic radius [$r(Sr^{2+}, CN = 12)$ = 1.44 Å] than Ba^{2+} [$r(Ba^{2+}, CN = 12)$ = 1.61 Å].[23]

The XRD patterns obtained from each compound allow the determination of their cell parameters with AFFMA[24], a program used in the calculation of cell parameters and assignation of Miller indices. Cubic BST50 (PDF 00-039-1395) and tetragonal BTO (PDF 00-005-0626) were used as a reference in the calculation input.

	Compound	*a* [Å]	*b* [Å]	*c* [Å]	Volume [Å^3]	Density [g cm^{-3}]
1	**BTO**	3.9933(5)	3.9933(5)	4.0306(5)	64.27	6.02
2	**BST50**	3.9473(4)	3.9473(4)	3.9473(4)	61.50	5.62
3	**BST60**	3.9406(2)	3.9406(2)	3.9473(4)	61.19	5.52
4	**BST70**	3.9256(9)	3.9256(9)	3.9473(4)	60.49	5.45

Table 3. Cell parameters of cubic BST.

The data present in Table 3 confirm the correlation between the increase of the cell volume and the Sr content, as represented in Figure 17. In addition, all compounds have a unit cell with an angle of 90 °, which is the expected value for tetragonal and cubic symmetries.

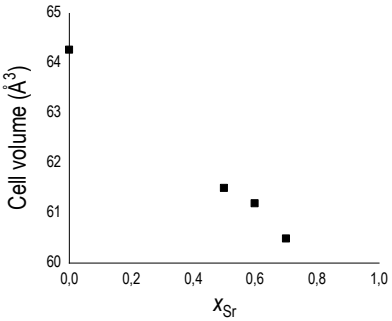

Figure 17. *Variation of cell volume with strontium content for the BST compounds.*

6.2. SCANNING ELECTRON MICROSCOPY – ENERGY DISPERSIVE X-RAY SPECTROSCOPY

Images obtained by SEM were taken with 4500× magnification. The surface of the BTO and BST sintered samples were analysed through secondary electrons, obtaining information about the morphology of the grains, backscattered electrons, obtaining information about the homogeneity of the sample, and EDS, which gives information on the composition of the sample.

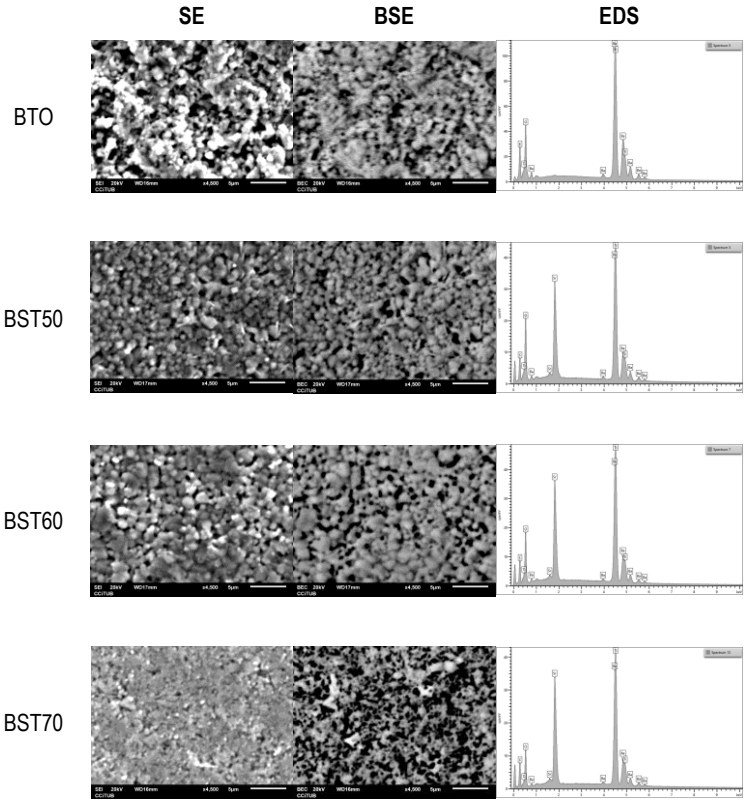

Figure 18. *Secondary and backscattered electrons images and EDS of BTO and BST compounds.*

SE images on Figure 18 show the porosity of the samples. It can be seen that size of BST grains decreases with the increase of Sr^{2+} concentration.

BSE images display the formation of a homogeneous phase. Moreover, EDS confirms the presence of Ba, Sr and Ti, along with the variation of the sample composition due to the Ba/Ti and Sr/Ti intensity ratio.

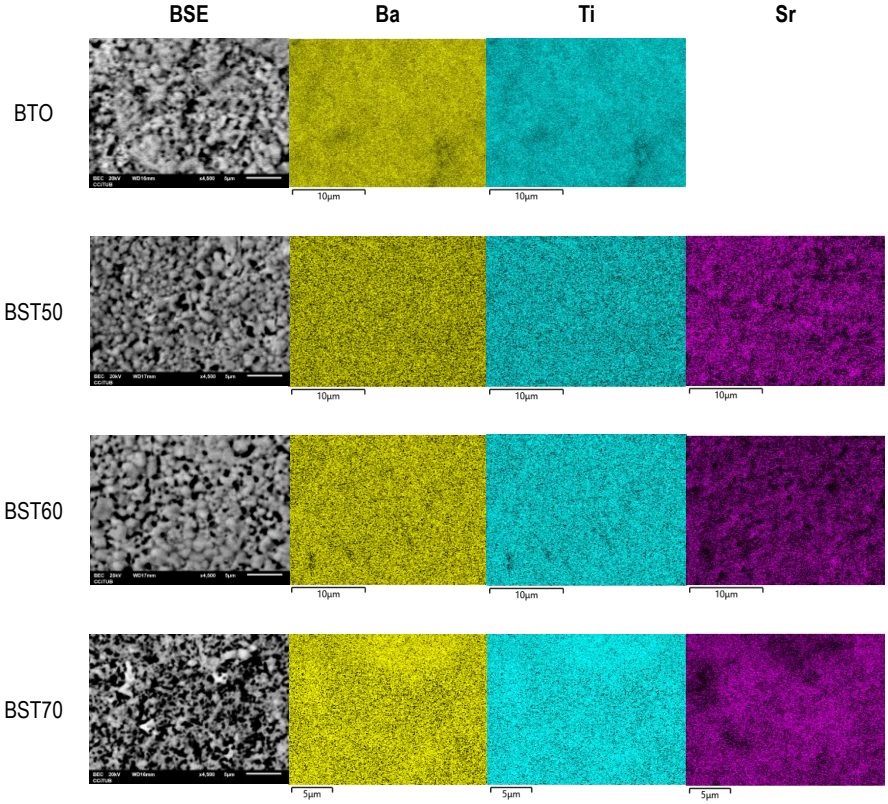

Figure 19. BSE images and *distribution of the elements present in the BTO and BST samples.*

Additionally, the distribution of the elements present in each compound was analysed, as seen in Figure 19. It can be appreciated that BST50 and BST60 have a homogeneous distribution of Ba^{2+} and Sr^{2+}, whereas the BST70 sample presents regions with low Sr concentration. No major impurities were observed in the samples.

6.3. ELECTROCHEMICAL IMPEDANCE SPECTROSCOPY

Phase transitions of barium titanate and barium strontium titanate were characterised by the measurement of relative permittivity and dielectric loss at different frequencies as a function of temperature. The result of BTO is shown in Figure 20.

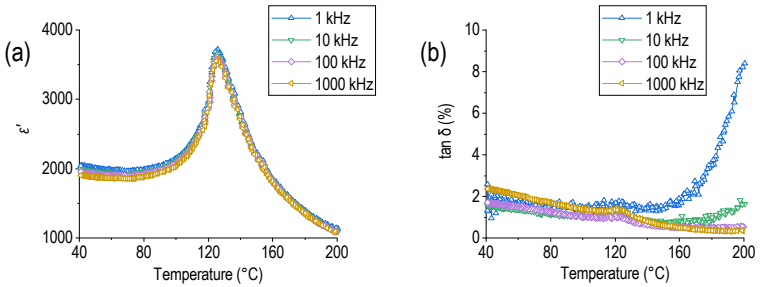

Figure 20. *Temperature dependence of permittivity (a) and dielectric loss (b) of BTO at different frequencies.*

It can be seen in Figure 20a that BTO permittivity peaks with $\varepsilon' = 3660$ at 126 °C, the temperature where the tetragonal-cubic transition takes place, due to the tetragonal phase being ferroelectric and the cubic paraelectric. This behaviour is caused by the hysteresis present in the sample, provoked by the displacement of atoms from their equilibrium position. The only way to prevent this is by giving atoms enough time to return to the equilibrium position. This is only possible with the performance of an electrical characterisation where the temperature is increased at $\Delta T \rightarrow 0$ during a time interval $t \rightarrow \infty$.

The sharp permittivity peak indicates that the tetragonal-cubic transformation is a normal phase transition. Additionally, it can also be observed that frequency variation has no influence on the value of permittivity. It is also seen that BTO presents small dielectric losses at temperatures below the permittivity maximum at T_C. In the tetragonal phase, tan δ decreases as T_C is approached. However, in the cubic phase, dielectric losses increase with temperature.

This electrical characterisation was also performed with BST compounds, as shown in Figures 21 to 23.

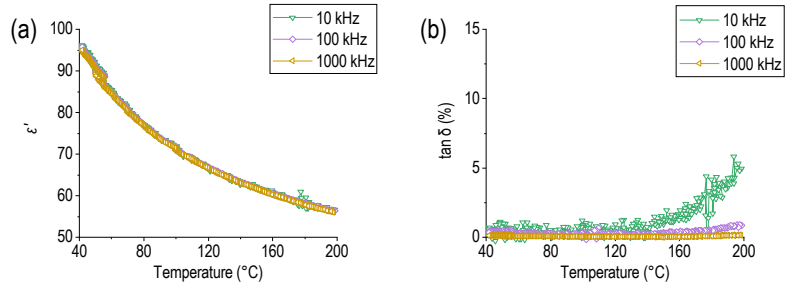

Figure 21. *Temperature dependence of permittivity (a) and dielectric loss (b) of BST50 at different frequencies.*

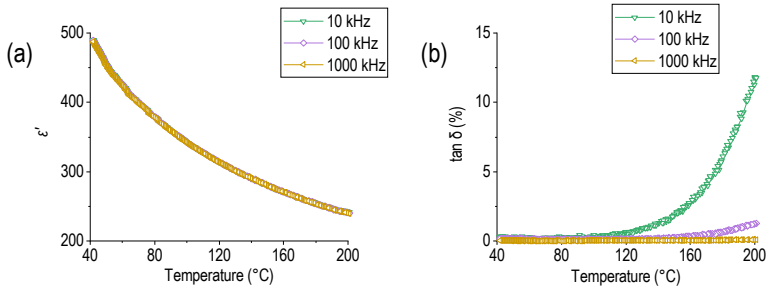

Figure 22. *Temperature dependence of permittivity (a) and dielectric loss (b) of BST60 at different frequencies.*

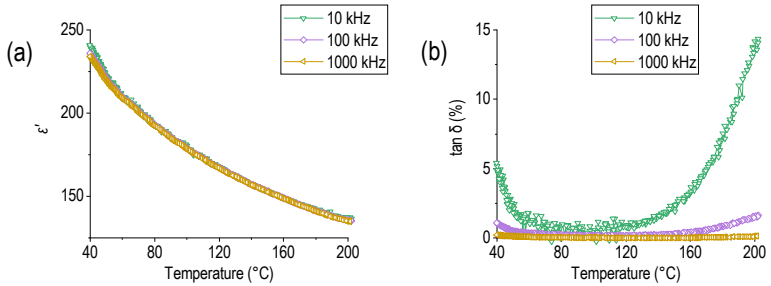

Figure 23. *Temperature dependence of permittivity (a) and dielectric loss (b) of BST70 at different frequencies.*

It can be seen on all three compounds that permittivity decreases with temperature for all frequencies, while a peak like the one seen in Figure 20a for BTO never takes place. This phenomenon happens due to BST being in the cubic phase and therefore its phase transition being out of the studied temperature range. The cubic-tetragonal phase transition should be found at $T < 40$ °C, since lowering the temperature increases the permittivity.

BST compounds present low dielectric losses, especially at $T < 126$ °C, which means that all compounds are good dielectrics.

The dependence of permittivity and dielectric losses with the composition of BST at a fixed frequency is represented in Figure 24.

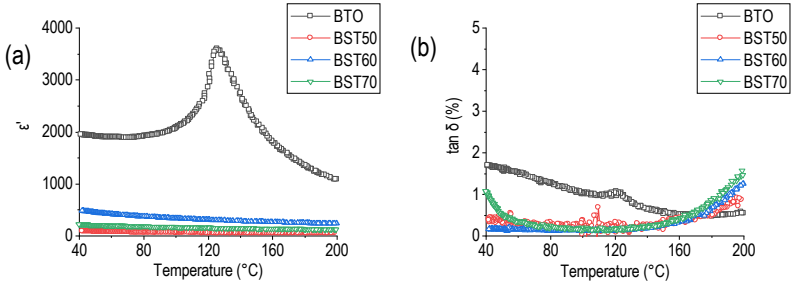

Figure 24. *Temperature dependence of permittivity (a) and dielectric loss (b) of BTO and BST at 100 kHz.*

It is seen in this region of temperatures that compounds with a bigger content of Sr have a smaller permittivity. Nevertheless, permittivity shows small variability for this range of temperatures, in contrast with BTO.

Additionally, it is seen that dielectric losses of BST compounds are lesser than those of BTO for temperatures between 40 °C and 160 °C, which implies that BST has a better dielectric behaviour than BTO at the studied temperature interval.

7. CONCLUSIONS

The ceramic method is a simple yet effective method of obtaining dense solid samples of the desired stoichiometry. An accurate weighting is crucial in the obtention of a product with exact composition. A dense and single-phase BTO and BST product was obtained after continuous thermal treatment cycles. For this to be possible, calcination at 1250 °C and sintering at 1350 °C are favourable conditions.

The analysed BST compounds do not present phase transition in the studied temperature interval, which is a behaviour in concordance with the identified cubic structure. Permittivity of BST compounds has limited variability with temperature in the studied range, in contrast with the great fluctuation observed in BTO. Dielectric loss in BST is lesser than BTO for temperatures between 40 °C and 160 °C.

Dielectric behaviour in BST70 was slightly deviated from the tendency observed in the other BST compounds, which could be caused by compositional inhomogeneities observed by SEM/EDS.

BST compounds are strong candidates to be used for high-energy store capacitors.

8. REFERENCES AND NOTES

1. A century of ferroelectricity. *Nature Materials,* **2020**, *19*, 129.
2. Valasek, J. Piezo-Electric and Allied Phenomena in Rochelle Salt. *Physical Review,* **1921**, *17*, 475.
3. Busch, G. *et al*. Eine neue seignette-elektrische Substanz. *Naturwissenschaften,* **1935**, *23*, 737.
4. Hippel, A. von, *et al*. High dielectric constant ceramics. *Industrial & Engineering Chemistry,* **2002**, *38*, 1097.
5. Jaffe, H. Titanate Ceramics for Electromechanical Purposes. *Industrial & Engineering Chemistry,* **1950**, *42*, 264.
6. Acosta, M. *et al*. $BaTiO_3$-based piezoelectrics: Fundamentals, current status, and perspectives. *Applied Physics Reviews,* **2017**, *4*, 041305.
7. Rödel, J. *et al*. Transferring lead-free piezoelectric ceramics into application. *Journal of the European Ceramic Society,* **2015**, *35*, 1659.
8. Rao, C. N. R. *et al*. *New directions in solid state chemistry*. (Cambridge University Press, 1997).
9. West, A. R. *Basic solid state chemistry*. (John Wiley & Sons, 1999).
10. King, G. *et al*. Cation ordering in perovskites. *Journal of Materials Chemistry,* **2010**, *20*, 5785.
11. West, A. R. *Solid state chemistry and its applications*. (John Wiley & Sons, 1984).
12. Lemanov, V. *et al*. Phase transitions and glasslike behavior in $Sr_{1-x}Ba_xTiO_3$. *Physical Review B,* **1996**, *54*, 3151.
13. Ban, Z.-G. *et al*. Phase diagrams and dielectric response of epitaxial barium strontium titanate films: A theoretical analysis. *Journal of Applied Physics,* **2002**, *91*, 9288.
14. Ioachim, A. et al. Transitions of barium strontium titanate ferroelectric ceramics for different strontium content. *Thin Solid Films,* **2007**, *515*, 6289.
15. Zhang, L. *et al*. The cell volume effect in barium strontium titanate. *Solid State Communications,* **1997**, *104*, 263.
16. Zhou, L. *et al*. Dependence of the Structural and Dielectric Properties of $Ba_{1-x}Sr_xTiO_3$ Ceramic Solid Solutions on Raw Material Processing. *Journal of the European Ceramic Society,* **1999**, *19*, 2015.
17. Garten, L. M. *et al*. Relaxor Ferroelectric Behavior in Barium Strontium Titanate. *Journal of the American Ceramic Society,* **2016**, *99*, 1645.
18. von Hauff, E. Impedance Spectroscopy for Emerging Photovoltaics. *Journal of Physical Chemistry C,* **2019**, *123*, 11329.
19. Lvovich, V. F. *Impedance spectroscopy: Applications to electrochemical and dielectric phenomena* (John Wiley & Sons, 2012).
20. Goldstein, J. I. *et al*. *Scanning Electron Microscopy and X-ray Microanalysis*. (Springer US, 2003).
21. Rojac, T. *et al*. The formation of a carbonato complex during the mechanochemical treatment of a Na_2CO_3–Nb_2O_5 mixture. *Solid State Ionics,* **2006**, *177*, 2987.
22. Socrates, G. Infrared and Raman characteristic group frequencies. Tables and charts. (John Wiley & Sons, 2001).
23. Shannon, R. D. Revised effective ionic radii and systematic studies of interatomic distances in halides and chalcogenides. *Acta Crystallographica Section A,* **1976**, *32*, 751.
24. Stewart, AFFMA, Affinement des Paramètres de Maille, modified by Rodriguez-Carvajal, J. (1985).

12. ACRONYMS

BST*x*: Barium strontium titanate ($Ba_{1-x}Sr_xTiO_3$)

BTO: Barium titanate ($BaTiO_3$)

EDS: Energy dispersive X-ray spectroscopy

EIS: Electrochemical impedance spectroscopy

PZT: Lead zirconate titanate ($PbZr_xTi_{1-x}O_3$)

SEM: Scanning electron microscopy

XRD: X-ray diffraction